



Journal of Geophysical Research: Solid Earth

RESEARCH ARTICLE

10.1029/2018JB015783

Key Points:

- Evidence from seismic anisotropy suggests the existence of a tear in S Cocos slab
- The rollback process of the slab is a key element for the abrupt end of the TMVB
- The slab window may create a corner flow for the isolated volcanoes in S Mexico

Supporting Information:

- Supporting Information S1
- Table S1
- Table S2

Correspondence to: J. C. Castellanos, jacastil@caltech.edu

Citation:

Castellanos, J. C., Clayton, R. W., & Pérez-Campos, X. (2018). Imaging the eastern Trans-Mexican Volcanic Belt with ambient seismic noise: Evidence for a slab tear. Journal of Geophysical Research: Solid Earth, 123, 7741–7759. https://doi.org/10.1029/2018.IB015783

Received 16 MAR 2018 Accepted 18 AUG 2018 Accepted article online 22 AUG 2018 Published online 13 SEP 2018

O2018. The Authors.

This is an open access article under the terms of the Creative Commons

Attribution-NonCommercial-NoDerivs
License, which permits use and distribution in any medium, provided the original work is properly cited, the use is non-commercial and no modifications or adaptations are made.

Imaging the Eastern Trans-Mexican Volcanic Belt With Ambient Seismic Noise: Evidence for a Slab Tear

Jorge C. Castellanos 10, Robert W. Clayton 10, and Xyoli Pérez-Campos 20

¹ Seismological Laboratory, Department of Earth and Planetary Sciences, California Institute of Technology, Pasadena, CA, USA, ²Instituto de Geofísica, Universidad Nacional Autónoma de México, Mexico City, Mexico

Abstract The eastern sector of the Trans-Mexican Volcanic Belt (TMVB) is an enigmatic narrow zone that lies just above where the Cocos plate displays a sharp transition in dipping angle in central Mexico. Current plate models indicate that the transition from flat to steeper subduction is continuous through this region, but the abrupt end of the TMVB suggests that the difference in subduction styles is more likely to be accommodated by a slab tear. Based on a high-resolution shear wave velocity and radial anisotropy model of the region, we argue that a slab tear within South Cocos can explain the abrupt end of the TMVB. We also quantify the azimuthal anisotropy beneath each seismic station and present a well-defined flow pattern that shows how mantle material is being displaced from beneath the slab to the mantle wedge through the tear in the subducted Cocos plate. We suggest that the toroidal mantle flow formed around the slab edges is responsible for the existence of the volcanic gap in central Mexico. Moreover, we propose that the temperature increase caused by the influx of hot, less dense mantle material flowing through the tear to the Veracruz area may have significant implications for the thermomechanical state of the subducted slab and explain why the intermediate-depth seismicity ends suddenly at the southern boundary of the Veracruz basin. The composite mantle flow formed by the movement of mantle material through the slab tears in western and southern Mexico may be allowing the Cocos plate to roll back in segments.

Plain Language Summary The Trans-Mexican Volcanic Belt (TMVB) is a prominent and enigmatic feature of the subduction system in Mexico. Its volcanic style diversity and oblique orientation to the trench are explained by the large along-strike variations in the subduction parameters of the Rivera and Cocos plates. However, the abrupt termination of the TMVB on its eastern end with the Pico de Orizaba volcano is puzzling as the current slab model suggests that the transition of the Cocos flat-slab geometry to normal subduction is smooth through this region. There is evidence that suggests that a tear in the slab might be developing, but it is unclear how this feature can support the unusually large topographic gradient that connects the volcanic high peaks with the Veracruz basin just south of the volcanic front. To provide further insight into the transition anatomy of this portion of the subducted slab and its relation with surface topography, we present a detailed and unified model of the velocity structure of the crust and uppermost mantle of central Mexico.

1. Introduction

The Trans-Mexican Volcanic Belt (TMVB) is one of the largest volcanic arcs on the North America plate. This Neogene continental arc grows over the central Mexican margin of the North American Plate, as a result of the subduction of the Rivera and Cocos plates along the Middle America Trench (MAT) and is composed of nearly 8,000 igneous structures that extend from the coast of Jalisco to the Gulf of Mexico in Veracruz (Demant, 1978; Figure 1). The remarkable compositional variability of the TMVB and its unusual lack of parallelism to the trench are unique aspects of the Central America tectonics that have been extensively debated over the years. Today, however, geophysical evidence indicates that the Rivera and Cocos oceanic plates are being subducted with highly variable dip angles that explain the obliquity of the volcanic arc (Gómez-Tuena et al., 2006).

In the present-day configuration, the western sector of the TMVB overrides the Rivera microplate, whereas the central and eastern sectors are underlain by the Cocos plate. Slab contours determined by precise hypocentral localization show that the Rivera plate dips at a steep and constant angle of \sim 50° beneath the Jalisco block and that earthquakes extend to a depth of \sim 120 km (Pardo & Suarez, 1995). Conversely, in central Mexico, the Cocos plate exhibits marked changes in its geometry and seismicity does not exceed \sim 80-km depth (Suárez

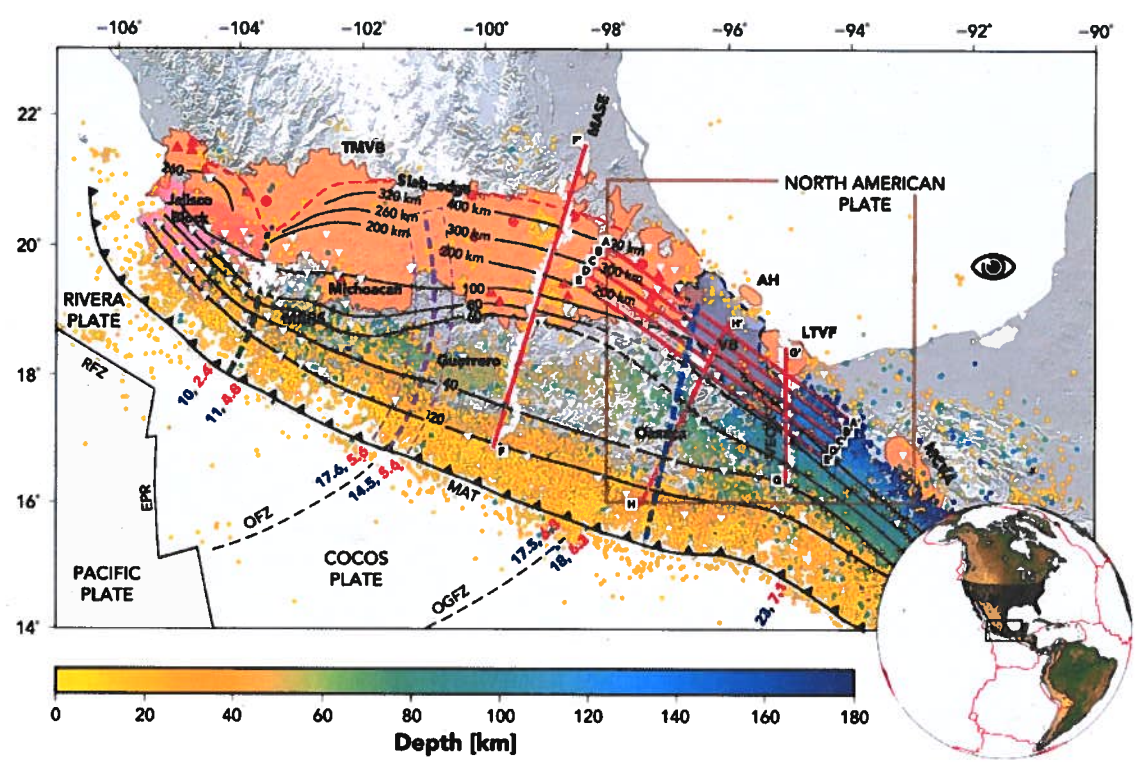


Figure 1. Tectonic setting of central and southern Mexico. The brown box indicates the main focus area of this study. The black contour lines depict the depth of the subducted slab compiled using the results of receiver functions, tomography studies, and hypocentral relocalization (from Ferrari et al., 2012). The dashed part of these contour lines indicates the transition between the flat and normal dipping portion of the South Cocos plate. The inverted white triangles show the location of the broadband seismic stations that have operated within this region. Regional seismicity at different depths, as reported by the Servicio Sismológico Nacional (SSN) since 1998, is shown as color-coded circles. The volcanic provinces: the Trans-Mexican Volcanic Belt (TMVB), the Anegada High (AH), the Los Tuxtlas Volcanic Field (LTVF), and the Modern Chiapanecan Volcanic Arc (MCVA) are delimited by the orange areas, and the location of the main stratovolcanoes and calderas are marked by the red triangles and red circles, respectively. The light purple region delimits the Veracruz Basin (VB), and the light magenta region delimits the Jalisco Block. The green dashed line denotes the Rivera-Cocos plate boundary, and the purple dashed line denotes the projected path of the Orozco Fracture Zone (OFZ) beneath North America (Dougherty et al., 2012). The blue dashed line indicates the location where the slab exhibits a significant change in dip and where Dougherty and Clayton (2014) propose the existence of a trench-perpendicular tear. The ages of the plates (Ma) and the convergence rates (cm/year) along the Middle America Trench (MAT) are shown in blue and red numbers, respectively. The inset map shows this work study area and the distribution of every station used in this study.

& Sánchez, 1996). Beneath the Michoacán area (from 103° to 102°W), the Cocos plate displays a shallow slab dip that gradually decreases eastward under Guerrero (from 102° to 98°W), where the slab is subhorizontal for about 250 km (Pardo & Suarez, 1995). From 98°W, the slab dip increases eastward until reaching a uniform angle of ~50–60° in central America (90°W) beneath Guaternala, El Salvador, Nicaragua, and Costa Rica (Arroyo et al., 2009; Husen et al., 2003; Syracuse et al., 2008).

More recent studies have refined the morphology of the Rivera and Cocos plates beneath the continent and investigated their relation with the particular space distribution of volcanoes along the convergent regime. Waveform modeling of moderate-size intraslab earthquakes recorded by the MARS (Mapping the Rivera Subduction Zone) experiment (Dougherty et al., 2012) and seismic anisotropy measurements (Stubailo et al., 2012) suggest that the Cocos slab could be currently fragmenting along the landward projection of the Orozco Fracture Zone (OFZ) by a similar process to that which occurred when the Rivera plate separated from the proto-Cocos plate (Bandy et al., 2000). This tear is proposed to indicate the ongoing fragmentation of the Cocos slab into North Cocos and South Cocos plates and would explain the observed offset of the volcanic arc in the Michoacán area (Dougherty et al., 2012). East of this region, receiver functions, and seismic velocity tomography along the MASE (MesoAmerican Subduction Experiment) line confirmed that the Cocos plate is subhorizontal in the Guerrero region and showed that the slab then plunges steeply into the mantle at a dip of ~75° where it is finally truncated at 500 km (Husker & Davis, 2009; Kim et al., 2010; Pérez-Campos et al.,

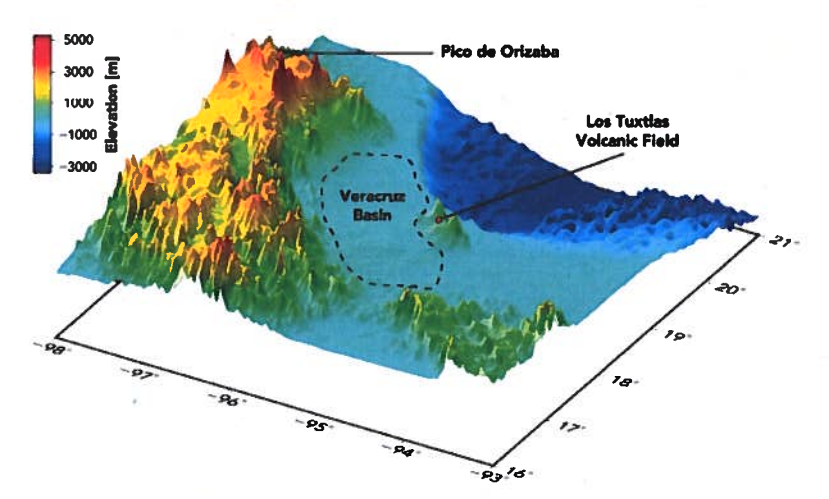


Figure 2. Elevation map of the eastern section of the Trans-Mexican Volcanic Belt showing the abrupt termination of the volcanic arc. Note how altitude drops more than 5,000 m from Pico de Orizaba to the coastal Veracruz basin over a horizontal distance of 120 km. This region corresponds to the one encompassed by the brown box in Figure 1.

2008). This atypical subduction geometry suggests that the slab is rolling back and forcing the volcanic arc to retreat (Pérez-Campos et al., 2008), as confirmed by the age progression of volcanism migrating trenchward (Ferrari, 2004). Further to the south, detailed analysis of receiver functions along the VEOX (Veracruz-Oaxaca) line indicates that the Cocos plate dips at a constant angle of ~26° to a depth of 150 km, where it appears to be truncated by an anomalous southwest dipping slab that extends to a depth of 250 km (Kim et al., 2011; Melgar & Pérez-Campos, 2011).

In between the MASE and VEOX experiments, near the transition from shallow to normal subduction, the TMVB ends abruptly with Pico de Orizaba. This stratovolcano is the highest point in Mexico and sits at the front of an active volcano chain that is oriented almost perpendicular to the trench. Coupled with this feature is an extremely sharp topographic gradient that connects the volcanic arc high peaks with the Veracruz basin (altitude drops ~5,000 m over a horizontal distance of just 120 km; Figure 2). Crustal thickness measurements derived from gravity data (Molina-Garza & Urrutia-Fucugauchi, 1993; Urrutia-Fucugauchi & Flores-Ruiz, 1996) and receiver functions (Espíndola et al., 2017) indicate that a simple isostasy compensation model is insufficient to explain the thickness difference between these two regions. Furthermore, the presence of the nearby late Miocene Anegada High submarine volcanic complex (Ferrari et al., 2005) and the active Los Tuxtlas Volcanic Field (LTVF) (Nelson et al., 1995) marks an interruption of arc volcanism that is thought to be associated with the steepening and rollback motion of the slab. However, the mechanisms of their origin remain unclear.

Altogether, these features indicate that the transition from shallow to normal subduction in central Mexico is more complicated than it was originally suggested in the Pardo and Suarez (1995) plate model. To account for the abrupt end of the TMVB, and the discontinuity of arc volcanism in central southern Mexico, Dougherty and Clayton (2014) propose the existence of a possible tear located within the downdip portion of the South Cocos plate. Conversely, patterns of local seismicity, tectonic tremor, and slow-slip events support the idea that a sharp flexure of the slab in both the downdip and along-strike directions accommodates the transition from flat to steeper subduction (Fasola et al., 2016). In this study, we determine the shear wave velocity structure and radial anisotropy of the upper crust and lithosphere in central Mexico by inverting Rayleigh and Love dispersion curves. In addition, we quantify the azimuthal anisotropy present beneath each seismic station using an array analysis to resolve variations in the direction of mantle flow in the region. The combined understanding of the velocity distribution and seismic anisotropy allows us to place constraints on the transition structure of the subducted slab and its relation with the abrupt end of the TMVB at its eastern limit.

2. Data and Method

The data used in this study consist of surface wave signals obtained from the three-component cross correlation of background noise recorded at over 2,000 broadband stations. This data set results from combining every available seismic network that operated within Mexico and its surroundings (from 5° to 40°N and -125°



to -60°E) from January 2006 to December 2016. For a detailed description of the stations involved in this study refer to Table S1 in the supporting information. The reader is also referred to Pérez-Campos et al. (2018) and Córdoba-Montiel et al. (2018) for a summary of the permanent stations in this area.

2.1. Ambient Noise Cross Correlations

Both theoretical and experimental studies have demonstrated that by cross correlating the ambient noise recorded at two stations over a sufficiently long period of time, the Green's function between the two stations can be retrieved (e.g., Campillo & Paul, 2003; Lobkis & Weaver, 2001; Sager et al., 2018; Shapiro & Campillo, 2004; Snieder, 2004). Here we use a technique very similar to the one described by Bensen et al. (2007) to compute the three-component cross correlations of continuous recordings between all synchronous station pairs. The single-station data preparation consists of (i) downsampling the records of all three components to one sample per second and dividing them into 1-day time windows, (ii) removing the mean and trend value in each time window, (iii) band-pass filtering between the 3- and 100-s period band, (iv) whitening the spectra, and (v) normalizing in the time domain. Once the preprocessing is complete, each time window is cross-correlated, normalized to unit peak amplitude, and averaged over time. The cross-correlation traces are then rotated from the east-north-vertical frame into the radial-transverse-vertical frame between all station pairs. To simultaneously determine all nine components of the Green's tensor, we follow Muir and Tsai (2017) and build the rotation matrix as $M = M_1 \otimes M_2$, where M_1 , are the three-component rotation matrices from the east-north-vertical to the radial-transverse-vertical frame for the individual stations, and @ is the Kronecker product. Finally, to enhance the signal-to-noise ratio (SNR), the causal and anticausal parts of the cross correlations are stacked to obtain the so-called symmetric cross correlations. This process gave rise to more than 136,000 noise correlation functions for each of the nine calculated components. As evidence of the effectiveness of the process described above, Figure 3 shows the ZZ, RR, ZR, and TT cross correlations as a function of interstation distance for the period band of 5-100 s. Prominent surface wave signals and various body wave arrivals are visible in all four component combinations.

2.2. Dispersion Measurements

For the 3- to 70-s period band, we apply an automated image transformation technique (Yao et al., 2006) to retrieve the Rayleigh and Love wave phase and group velocity dispersions from the ZZ, RR, ZR, and TT cross correlations. Three selection criteria are imposed before accepting a measurement at a certain period. First, the minimum interstation spacing is set to one wavelength (e.g., Luo et al., 2015). Second, the maximum phase and group velocity measurement deviation from the average dispersion curve is limited to 0.5 km/s. Third, the SNR threshold is empirically set to 5. Here we define the SNR by the ratio of the peak amplitude within a window containing the surface wave signal to the mean of the noise trailing the direct arrival window. Generally, the SNR decreases with interstation distance due to scattering and attenuation; however, the relaxed restriction of one wavelength for the shortest path still allows sufficient coverage to extend our measurements up to 70 s. Finally, to increase the robustness of our measurements and ensure a larger period coverage, we stack the ZZ, RR, and ZR dispersion curves for identical paths (e.g., Spica et al., 2017). For this last step, we introduce an additional selection criterion that requires that the standard deviation at every common period be smaller than 0.1 km/s.

2.3. Tomographic Inversion

The Rayleigh and Love interstation dispersion measurements are used to invert for phase and group velocity maps using the method of Barmin et al. (2001). But before formulating the tomographic problem, it is necessary to consider that the elongated shape of our study region limits the number of long-period trench-perpendicular raypaths to the MASE and VEOX lines only. To mitigate the uneven ray coverage at long periods, we choose to include distant stations into the inversion and project all crossing seismic rays to a relatively wide rectangular area (from 14° to 23°N and -107° to -90° E) so as to provide an appropriate azimuthal coverage. A fundamental disadvantage of this approach, however, is the assumption that all velocity anomalies are contained within the study region. To that end, all measurements are downweighted throughout the inversion according to the percentage of the ray that lies outside the target area. The size and extension of this area is chosen by trial and error until the inverted models show the minimal amount of smearing while preserving all first-order features when compared to velocity maps that are produced with wider boxes and coarser grids (Figure S1). To carry out the actual inversion, homogeneous maps are constructed on a $0.4^{\circ} \times 0.4^{\circ}$ regular grid across the study region and are defined relative to the average slowness observed at each period of interest. The optimal grid size is chosen empirically based on a resolvability test for the periods

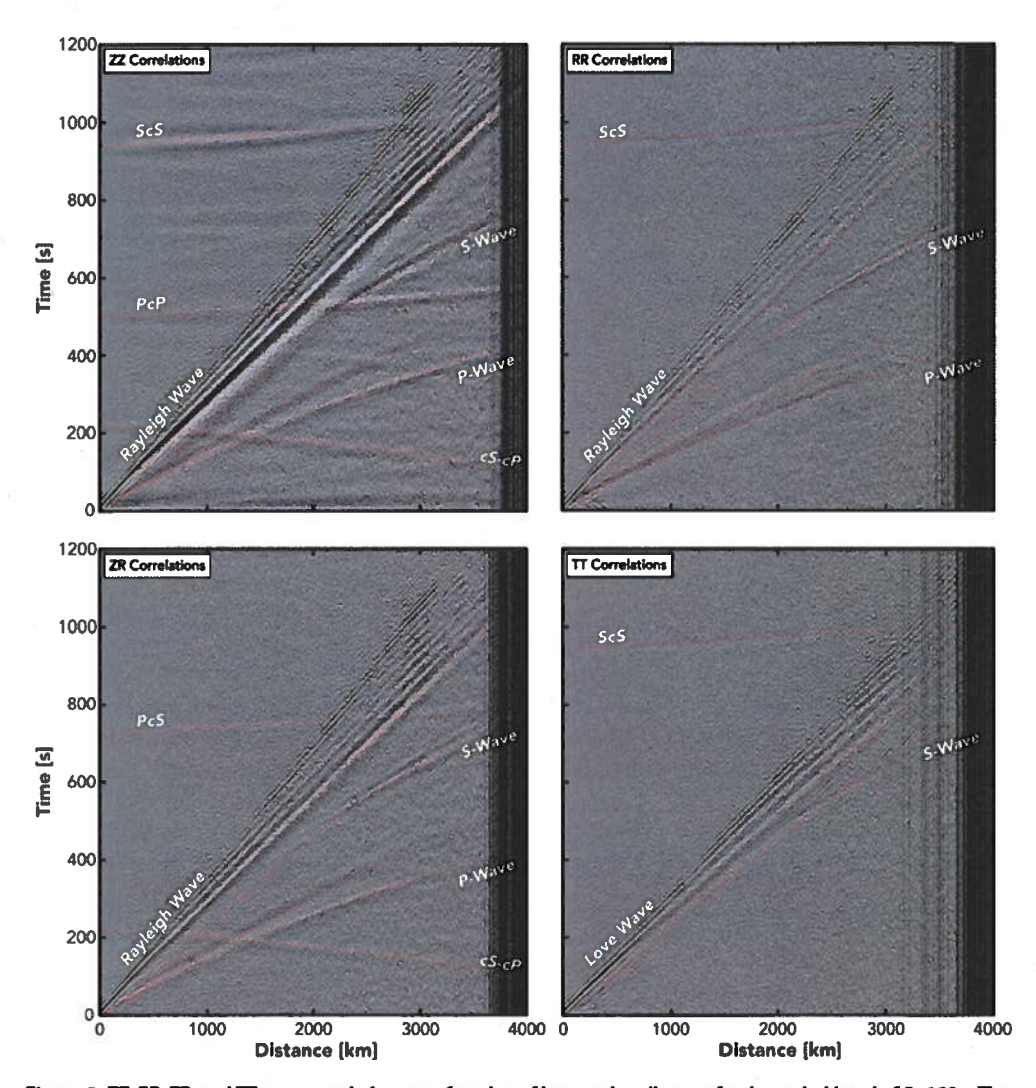


Figure 3. ZZ, RR, ZR, and TT cross correlations as a function of interstation distance for the period band of 5-100 s. The traces are stacked by bins of 2 km and 0.5 s. As expected, the extracted Green's functions show clear Rayleigh waves in the ZZ, RR, and ZR components and clear Love waves in the TT component; although several body wave arrivals emerge as well. Note the presence of the anomalous cS-cP core phase in the ZZ and ZR cross correlations (Pham et al., 2018).

with the lowest path density using Voronoi diagrams (Debayle & Sambridge, 2004). We then perform two full tomographic inversions. In the first inversion, no additional weights are added to the data and we apply heavy damping, which results in a highly smoothed model. Synthetic traveltimes are then computed and used to identify and discard highly anomalous measurements in the observations. A 3σ residual threshold is set for this criterion (e.g., Spica et al., 2016). For the second inversion, the remaining data are further downweighted according to their misfits in the first inversion and the optimum smoothing factor is determined from the misfit and model smoothness trade-off curve. The resulting slowness maps are then converted to phase and group velocity maps.

To assess the capability of the different raypath geometries to resolve for contrasting slowness distributions, we follow Ma and Clayton (2014) and use the resolution matrix $R = (G'C^{-1}G + Q)^{-1}G'C^{-1}G$ (where G is the generalized inverse or forward operator on the slowness model, C is the data covariance matrix, and Q is the regularization matrix) from the tomographic inversion to generate standard checkerboard resolution maps. For this test, we set up input models containing ± 1 -km/s perturbations and evaluate how accurately the tomography is able to retrieve the anomaly distribution. To characterize the error of the model, we use the

CASTELLANOS ET AL. 7745



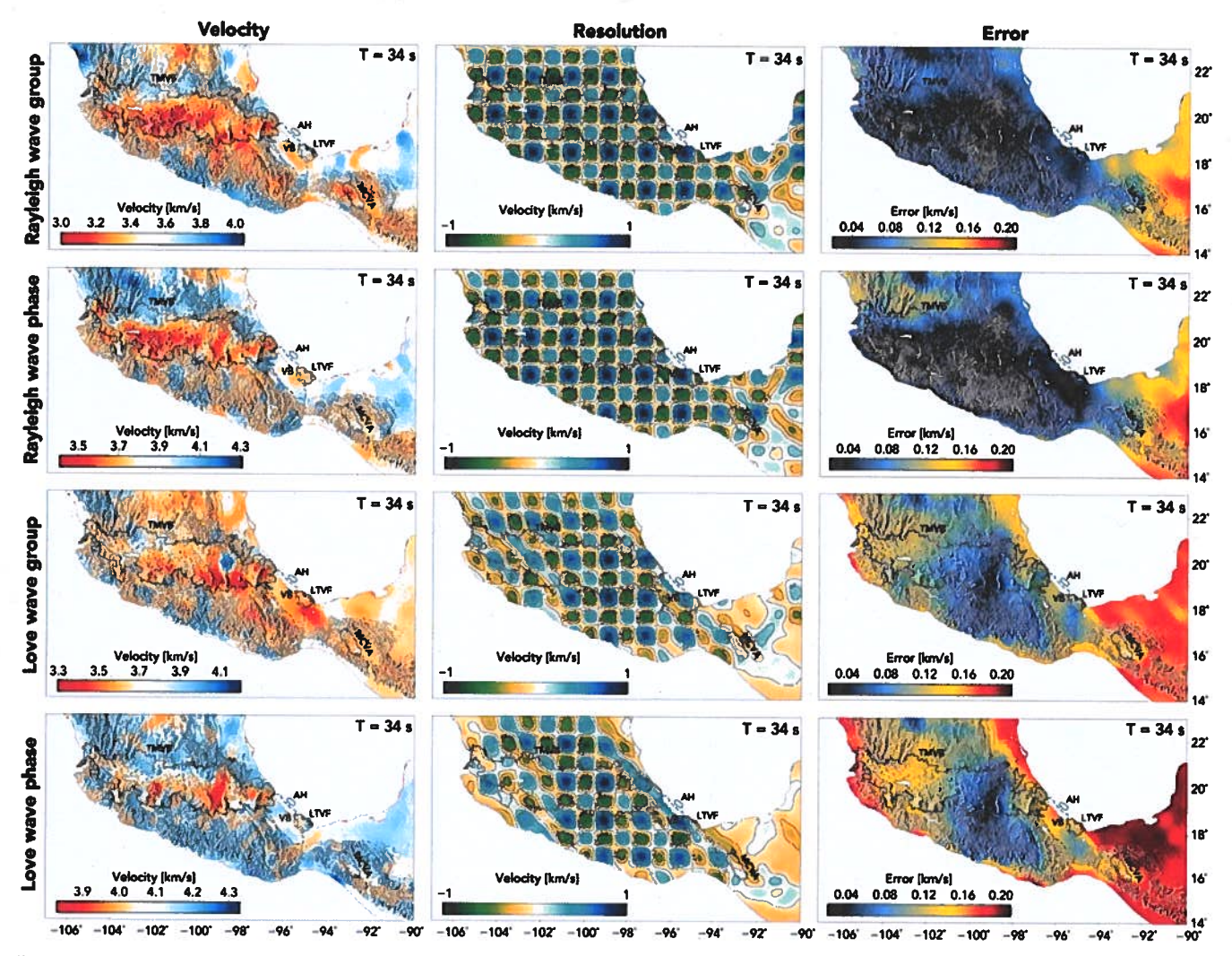


Figure 4. Ambient noise phase and group velocity maps (left column), checkerboard resolution maps (middle column), and model error maps (right column) at 34-s period. The volcanic provinces and the Veracruz Basin are delimited by the solid and dashed contour lines, respectively. Note how the velocity distribution varies for all four velocity types due to their difference in sensitivity.

diagonal elements of the model covariance matrix $C_{mm} = (G'C^{-1}G + Q)^{-1}$; which reflects the variance of the model subject to the variance of the data (Ma & Clayton, 2014).

As an example, Figure 4 shows the velocity maps, checkerboard resolution maps, and model error maps at 34-s period for both Rayleigh and Love surface waves. Perhaps the most important feature of these maps is that the velocity distribution varies for all four velocity types even though the measurements are taken at the same period. This can be explained by their differences in depth sensitivity and is the main reason why their joint analysis provides better constraints on the radial structure of the crust and lithosphere (e.g., Spica et al., 2017). Nonetheless, all models exhibit a similar pattern and reveal low velocities beneath the TMV8 (Figure 5). Based on the resolution maps, we find that the checkerboard structure is satisfactorily reproduced in all inversions except in the southeast sector of the study area. As expected, error along the coast is high, but it decreases to values smaller than 0.1 km/s as we approach central Mexico, where the path coverage in denser.

2.4. Inversion for Shear Wave Velocity and Radial Anisotropy

Once the velocity maps are constructed for each frequency, we extract the velocity dispersion curves at each (x, y)-point in the grid and use a linearized inversion algorithm (Ammon et al., 2004) to simultaneously map



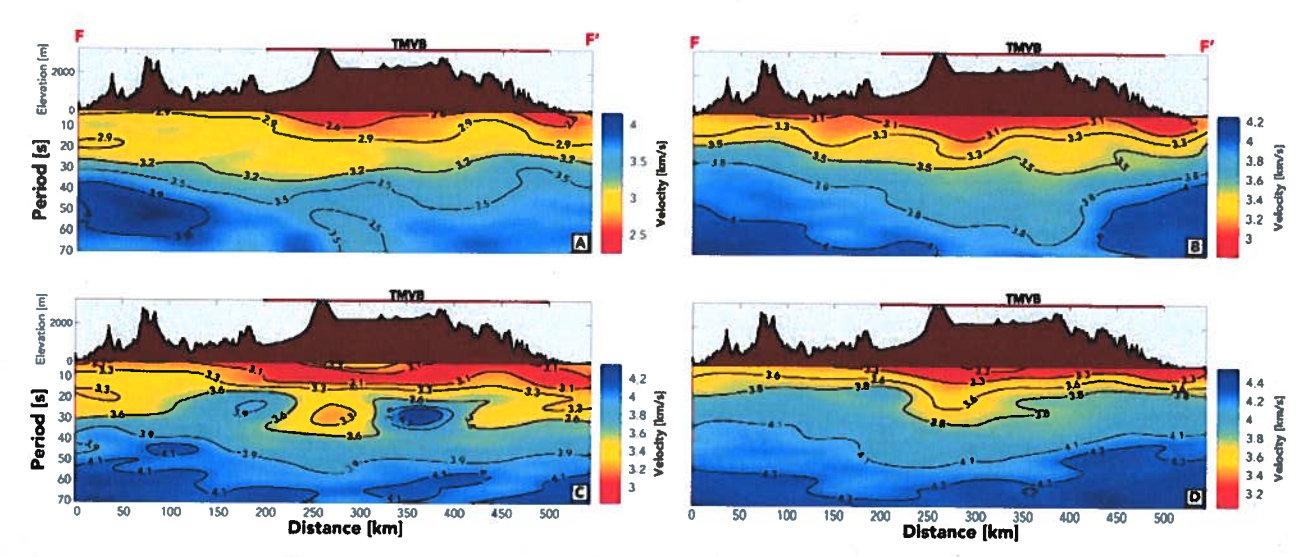


Figure 5. Cross sections of the Rayleigh wave group (a) and phase (b) velocity models and the Love wave group (c) and phase (d) velocity models along the MASE line (F-F' in Figure 1). Topography is shown above each profile. MASE = MesoAmerican Subduction Experiment.

the phase and group velocities as a function of period to shear wave velocity as a function of depth. This process is done independently for Rayleigh and Love waves to obtain a V_{SV} and a V_{SV} model, respectively.

For each inversion, we use a linearly increasing 1-D model discretized into 2-km layers at the top 50 km, then 5-km layers to 100 km, and finally 10-km layers to 140-km depth, as a starting model to solve for a smooth structure without a Moho discontinuity. The implications of not imposing a Moho in the inversion are addressed in Ma and Clayton (2014). We then assume a constant V_p/V_s ratio of 1.73 for the whole structure and determine the density from the compressional wave velocity (Gardner et al., 1974). Throughout the inversion, both the V_p/V_s ratio and density remain fixed and only the shear wave velocity is perturbed. The damping factor is chosen from the misfit and model smoothness trade-off curve. We also tested the case of reducing the damping factor with depth to account for the large heterogeneity of the uppermost crust but found no significant differences in the results. The final model is obtained by iteratively perturbing the initial model until a good fit to the two dispersion curves is achieved. Finally, we use regional average structures (1° × 1°) as initial models and perform one last inversion on a finer grid. For this step, each part of the dispersion curves is weighted inversely proportional to the model error in the tomographic inversions. The final 1-D velocity profiles are then combined to form two orthogonally polarized three-dimensional V_s models of the whole study region.

In a simple isotropic medium, both the V_{SV} and V_{SH} models would be identical, as shear waves travel at the same speed regardless of their polarization. However, in presence of variable tectonic stresses, complicated structures begin to emerge and reorient so that the shear wave velocity of the medium also depends on direction of propagation and polarization. The velocity dependence of the latter is termed radial anisotropy and is estimated here as

$$r = \frac{V_{\text{SH}} - V_{\text{SV}}}{V_{\text{c}}}.\tag{1}$$

where V_S is the isotropic or effective shear wave velocity and is directly computed from the V_{SV} and V_{SH} models via a Voigt's average:

$$V_{\rm S} = \sqrt{\frac{2V_{\rm SV}^2 + V_{\rm SH}^2}{3}}.$$
 (2)

The velocity distribution derived from equation (2) is then used to construct our final velocity model since it better reflects the apparent variations in elastic properties (Dziewonski & Anderson, 1981; Ekström & Dziewonski, 1998). Figure 6 shows vertical cross sections of our derived Voigt-averaged V_s and radial anisotropy model



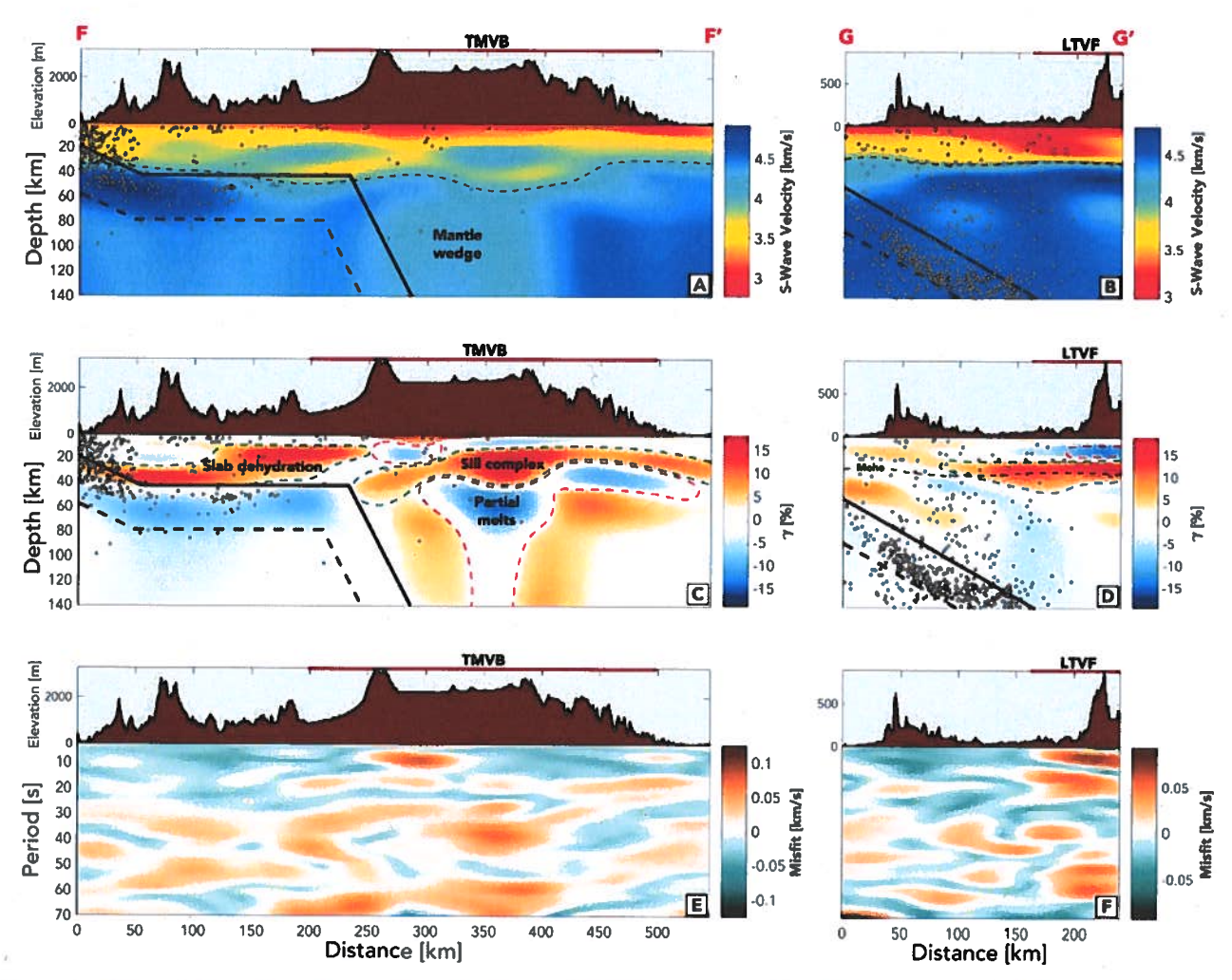


Figure 6. Vertical cross sections of the Voigt-averaged V_5 (a and b) and radial anisotropy models (c and d) along the MASE and VEOX lines (F-F' and G-G' in Figure 1, respectively). Topography is shown above each profile. The hypocenters from the SSN catalog within ± 10 km are projected to each cross section. The slab models from Pérez-Campos et al., 2008 (2008; for MASE) and Melgar & Pérez-Campos, 2011 (2011; for VEOX) are plotted in black lines assuming a constant plate thickness of 40 km. The thin black dashed line in profiles (a), (b), and (d) represent the Moho interface, defined by where the shear wave velocity first exceeds 4.1 km/s, and the thick green and red dashed lines in profiles (c) and (d) represent regions of elevated positive ($\geq V_{SH}$) and negative radial anisotropy ($> V_{SV}$), respectively. Cross-sections (e) and (f) show the average misfit of the 1-D inversion along the same profiles.

along the MASE and VEOX seismic lines (F-F' and G-G' in Figure 1, respectively) with their associated average misfits. An obvious feature in the $V_{\rm S}$ profiles is that superficial slow velocities correspond well with the TMVB and even more so for the LTVF, where the recently active San Martín Tuxtla Volcano is located. The radial anisotropy distribution, on the other hand, appears to be more contrasting and related to the subduction geometry. The main mechanisms responsible for causing radial anisotropy in a subduction environment, and how its presence can be interpreted, are addressed in section 3.

2.5. Inversion for Azimuthal Anisotropy

To characterize the azimuthal anisotropy, or the dependence of wave speed with azimuth of propagation, we adopt a beamforming approach and fit the first three parameters in Smith and Dahlen (1973) anisotropy model for Rayleigh waves:

$$v(T,\theta) = a_0(T) + a_1(T)\cos(2\theta) + a_2(T)\sin(2\theta) + a_3(T)\cos(4\theta) + a_4(T)\sin(4\theta), \tag{3}$$

where v is the surface wave phase velocity, T the period, θ the back azimuth, a_0 the isotropic velocity, and a_{1-4} the azimuthal coefficients (Backus, 1970), to the ZZ cross correlations. Only the isotropic and 2θ coefficients

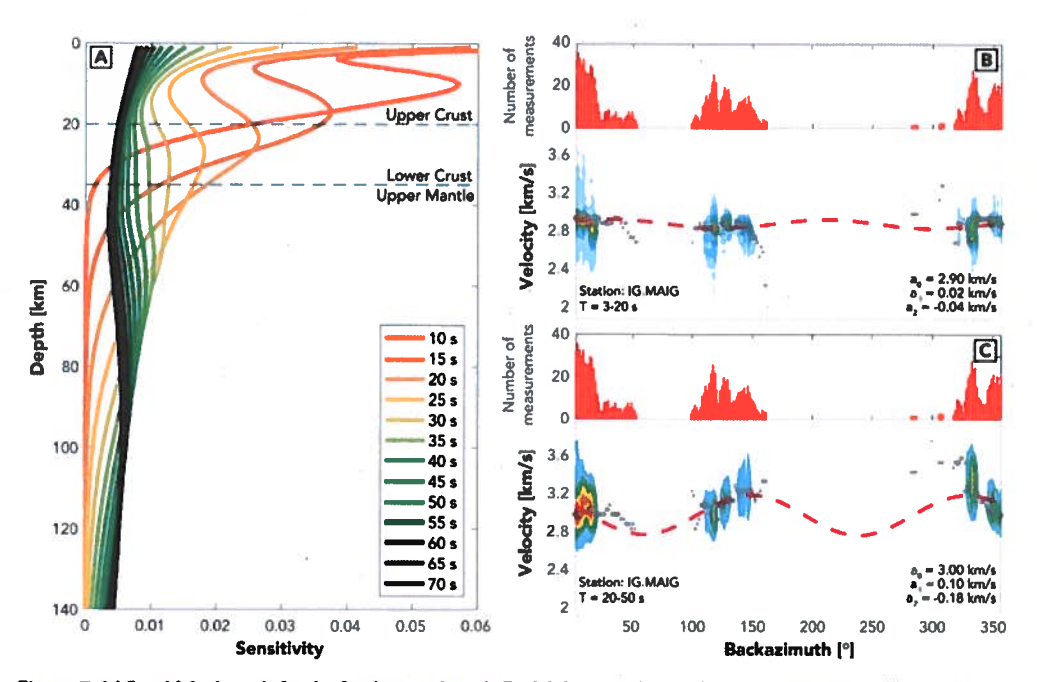


Figure 7. (a) Sensitivity kernels for the fundamental mode Rayleigh wave phase velocity calculated from the modified Tectonic North America Model (Stubailo et al., 2012). Two-dimensional histograms over the backazimuth-phase velocity space for the (b) 3- to 20-s period band, and the (c) 20- to 50-s period band. The orange bars on top of each panel represent the number of cross correlations beamformed in each backazimuth bin. The dashed red line indicates the best fit of equation (3), and the gray diamonds mark the beam velocity in each bin (with size as a function of beam power). The best fitting parameters are given at the bottom right of each panel.

are considered here because of the very small contribution that came from the rest of the parameters in our initial inversion. After characterizing the wavefield's azimuthal dependence at every station, we calculate the amplitude of the anisotropy, A, and its seismically fast direction, ϕ , using

$$A = \sqrt{a_1^2 + a_2^2},\tag{4}$$

$$\phi = \frac{1}{2} \arctan \frac{a_2}{a_1}.$$
 (5)

In the traditional beamforming method, one inverts the phase information by finding the best fitting slowness and back azimuth of a plane wave, thus providing a detailed characterization of the seismic wavefield at a given location (e.g., Harmon et al., 2008). Here we isolate stations one at a time, and use the remainder as virtual sources to find the average phase velocity of Rayleigh waves traveling to the reference station from all available azimuths. To ensure the robustness of our measurements, we only beamform cross correlations with a broadband SNR higher than 10 and an interstation distance larger than one wavelength of the lowest period of the band-pass filters. We also assume that the wavefield's full azimuthal dependance can only be characterized if the azimuth range of 180° is sampled by at least three paths in a five-bin range (Debayle & Sambridge, 2004). In the actual beamforming process, we search for the maximum coherent output over velocities from 1 to 5 km/s and every 5° from 0 to 360° back azimuth with 70% overlap for the 3- to 20- and 20- to 50-s period bands. Such period bands are determined empirically based on the Rayleigh wave phase velocity sensitivity to perturbations in V_5 in an effort to characterize the upper crust anisotropy and the lower crust and upper mantle anisotropy independently (Figure 7a). The sensitivity kernels are computed using the modified Tectonic North America Model (mTNA; Stubailo et al., 2012).

A visual inspection of Figures 7b and 7c clearly shows that the surface wave phase velocity varies with back azimuth differently over the two frequency bands. To find the best fitting coefficients to these variations, we perform a grid search using a weighted L2 regularization in which each azimuth bin is weighted proportionally to the amount of energy that was beamformed. The resulting best fits for two different frequency bands

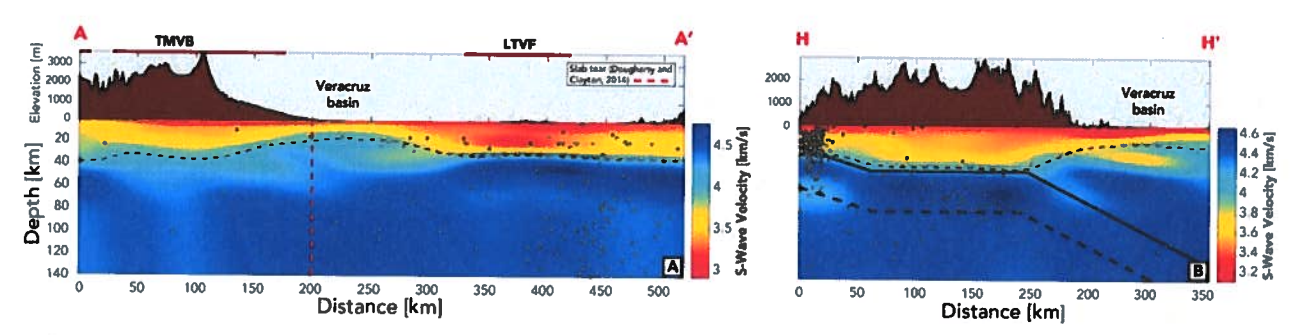


Figure 8. Vertical cross sections of the Voigt-averaged V_5 model along the A-A' and H-H' lines in Figure 1. Both profiles show extreme crustal thinning in the Veracruz basin. The dashed red line in panel (a) indicates the location where Dougherty and Clayton (2014) propose the existence of a plate tear. Topography is shown above each profile. Other symbols are as in Figures 6a and 6b.

are shown in Figures 7b and 7c as dashed red lines with the best fitting parameters given at the bottom right. A possible source of error in our procedure may come from the inherent trade-off between seismic heterogeneity and azimuthal anisotropy. However, given the broad frequency bands we make our measurements in, it is reasonable to assume that any effect caused by lateral heterogeneities will be minimal when compared to the one introduced by large-scale tectonic processes. To validate this assumption, we compare a stacked map of all the detrended Rayleigh wave phase velocity maps for the 20- to 50-s period band with the results of our beamforming process in the same period band for a given station in central Mexico (Figure S2). The comparison shows clear systematic velocity variation as a function of back azimuth with no direct correlation with the isotropic velocity distribution. Lastly, to assess the uncertainty in our fit parameters as well as their statistical significance, we estimate the 95% bootstrap confidence limits using 100 resamples. A table with the retrieved anisotropy parameters, their confidence limits, and associated L2 misfits is presented in Table S2.

3. Results and Discussion

3.1. Shear Wave Velocity and Radial Anisotropy

The shear wave velocity structure in central and southern Mexico has been discussed in a number of seismic imaging studies (e.g., Córdoba Montiel et al., 2014; Gaite et al., 2012; Spica et al., 2016). However, the enhanced ray coverage that is now provided by the GECO, OXNET, Veracruz, and expanded SSN networks allows us to resolve new features of the continental crust and uppermost mantle that were averaged out due to insufficient resolution, particularly at the eastern sector of the TMVB. Figures 8 and 9 show the results of our three-dimensional V_s model near the coastal Veracruz basin. Among the most striking features observed in the profiles of Figure 8 is the dramatic variation in crustal thickness that occurs in the transition of the TMVB and the LTVF, and how the crust thins out toward the Gulf of Mexico. Taking a 4.1 km/s limit in $V_{\rm S}$ as the crust and mantle transition zone (e.g., An et al., 2015), our results indicate that the Moho reaches a depth of about 45 km beneath the eastern TMVB and rises sharply to 20 km beneath the Veracruz basin just before lowering once more to an average depth of 40 km beneath the LTVF. Interestingly enough, this abrupt change in the Moho depth occurs just above where Dougherty and Clayton (2014) propose the existence of a plate tear and it encompasses the same ~50- to 75-km-wide zone where they observe a sharp decrease in intraslab seismicity (Figure 9). The crustal thickness measurements inferred from this study are, in general, consistent with previous experiments in the area (Espíndola et al., 2017; Molina-Garza & Urrutia-Fucugauchi, 1993; Urrutia-Fucugauchi & Flores-Ruiz, 1996). However, using a fixed velocity contour to define the Moho can be problematic if other physical processes that are altering the crust's chemistry are present.

In the shallow crust, radial anisotropy is thought to result from shape-preferred orientation in the form of fine layering, metamorphic foliations, and multiscale fractures in the crystalline rocks exposed to regional stresses (e.g., Fouch & Rondenay, 2006; Walker et al., 2004). Crystallographic-preferred orientation (CPO) of intrinsically anisotropic minerals can also cause strong anisotropy at shallow depths, but this mechanism seems to only be dominant in the upper mantle, where olivine and orthopyroxene aggregates are deformed during oriented geodynamic processes (Nicolas & Christensen, 1987). Anisotropy in the lower part of the continental crust generally does not have a strong seismic signature (Babuska & Cara, 1991). However, in subduction zone environments, significant radial anisotropy can be found in the overall crust and uppermost mantle arising from melt-filled cracks, lenses of partial melts, and other large-scale intrusive bodies such as dykes and sill

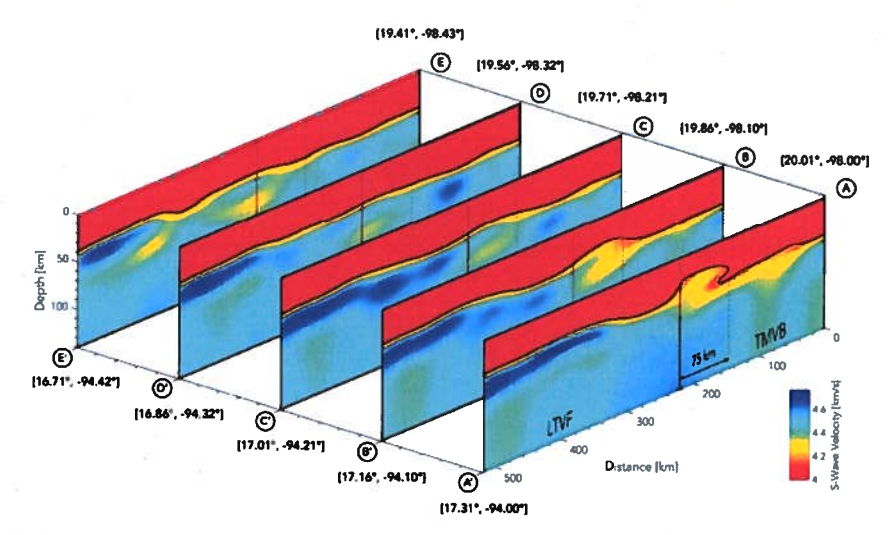


Figure 9. Vertical cross sections of the Voigt-averaged V_5 model in the Veracruz basin (from the A-A' to the E-E' lines in Figure 1). The color scale is saturated to only show the velocity anomalies present in the upper mantle. The solid black line indicates the Moho interface. The thick red line indicates the location where Dougherty and Clayton (2014) propose the existence of a plate tear, and the dashed red line delimits the 75-km-wide zone where they observe a sharp change in intraslab seismicity. Cross sections are separated by a constant offset of 20 km. The eye marker in Figure 1 indicates the viewpoint of the observer.

complexes (e.g., Jaxybulatov et al., 2014; Spica et al., 2017). The analysis of the strength and spatial extent of radial anisotropy can therefore be used to identify heterogeneous compositions in a wide range of depths. However, due to the potential biases in the background $V_{\rm SV}$ and $V_{\rm SH}$ velocities that arise from the difference in the regularizations imposed in the tomographic inversions, we limit the interpretation of our results to the changes in the sign of the radial anisotropy rather than the amplitude. An additional source of error in our radial anisotropy measurements may come from the leakage of Rayleigh wave energy in the TT components, which can be particularly strong at long periods and large interstation distances (Haney et al., 2012).

As previously stated, Figure 6c shows a complicated radial anisotropy pattern along the MASE line. A clear plume-like structure with negative radial anisotropy is present in the mantle wedge, where the V_S model predicts low velocities and the subducted plate starts diving into the continental mantle at a steep angle (Pérez-Campos et al., 2008). This feature is most likely related to the presence of partial melts and fluid upwelling since SV waves are traveling faster than SH waves in this zone. The ascent of this material appears to be confined to the base of the continental crust, at the point in our model where there is a sharp transition from negative to positive radial anisotropy. Considering that SV waves are being slowed in this part of the crust, we believe that this anisotropy contrast is due to the existence of molten material piled horizontally such as a large sill complex fed by the partial melts just beneath it. It is also worth noting a secondary positive radial anisotropic anomaly rooting-up from the flat portion of the Cocos plate. Although the cause of this anomaly is unclear, its location is coincident with where Jödicke et al. (2006) revealed a low resistivity zone that is related to the dehydration of the subducted slab. The slab itself, on the other hand, has a predominantly negative radial anisotropy that might reflect vertically oriented faults or fluid-filled cracks that are functioning as the primary conduit for slab dehydration. Interestingly enough, the zones with the highest negative anisotropy within the slab are close to the two patches in which tremors appear to occur regularly (the so-called sweet spot and transient zone (Cruz-Atienza et al., 2015; Husker et al., 2012)). This last observation is in agreement with previous receiver function results that revealed elevated shear wave splitting in these portions of the subducted oceanic crust along the MASE line (Castellanos et al., 2017).

Our radial anisotropy model along the VEOX line shows a marked negative anomaly beneath the LTVF (Figure 6d). This feature is commonly observed in volcanic environments and is probably related to the presence of a set of vertically oriented conduits or dikes that is storing the magma beneath the stratovolcanoes, such as the one Spica et al. (2017) imaged beneath the Colima volcano in Jalisco, southwestern Mexico. The source of the fluids and melts feeding the magma storage are unknown since the projected Cocos slab is far

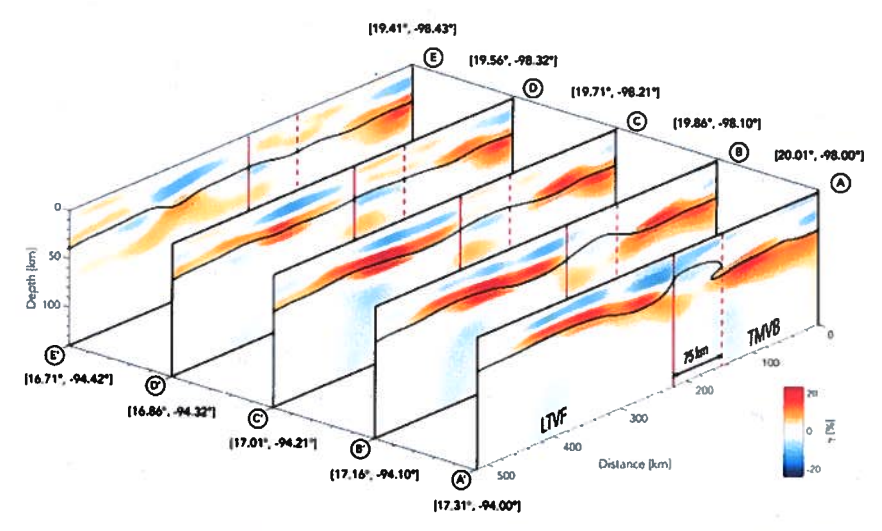


Figure 10. Vertical cross sections of the radial anisotropy model in the Veracruz basin (same profiles as in Figure 9).

too deep at this point to have an immediate effect on the overriding plate. We also do not find any evidence in the surface wave images of the anomalous south dipping structure seen in Kim et al. (2011) receiver function image. However, the isolated large positive radial anisotropy present in the 30- to 40-km-depth range beneath the LTVF indicates the possibility that melts are migrating laterally rather than being generated directly beneath the volcanoes. This observation is more intriguing in view of the fact that a magnetotel-luric profile collected at approximately 100 km west of the LTVF revealed an unresolved low-resistivity zone beneath the Veracruz basin (Jödicke et al., 2006). The radial anisotropy distribution along the VEOX line is a key element for establishing a relationship between the transition structure of the Cocos slab and the Central America volcanism and is discussed with more detail in section 3.3 of the paper.

Figure 10 shows the radial anisotropy along the same profiles as the ones presented in Figure 9. Although the anisotropy distribution appears to be smoother than the one observed along the MASE and VEOX experiments (where slab material is present at much shallower depths), there is a sharp positive radial anisotropy anomaly that delimits most of the crust-mantle transition zone. This observation is not too surprising since anisotropy in the uppermost mantle is generally governed by the systematic flow alignment of olivine crystals under dislocation creep, thus allowing SH waves to travel faster on average than SV waves (Anderson, 1965; Nicolas & Christensen, 1987). What is intriguing, however, is a subtle discontinuity in the anisotropic pattern at again, just above where Dougherty and Clayton (2014) propose the existence of a plate tear. This interruption in what appears to be the horizontal creeping flow of the mantle is indicative of a sharp structural change and may be related to some vertical flow component (e.g., West et al., 2009). Note that the lack of stations in and near the Gulf of Mexico may limit the resolution of these images.

3.2. Azimuthal Anisotropy

The slab rollback that has built the TMVB has proceeded a distance of 150 km over the past 20 Myr (Ferrari et al., 2001). This process requires a substantial movement of mantle material from the back to the front of the slab that can only be achieved by mantle flow beneath or around the subducted slab. Regardless of its path and orientation, this ductile flow is likely to produce a strong olivine CPO and lead to a bulk seismic anisotropy that should be observable at various scales. Under dry mantle conditions, the seismically fast olivine *a* axis generally aligns with the shear direction (Blackman & Kendall, 2002; Mainprice & Ildefonse, 2009). However, recent experimental work has shown that the presence of water in the medium can change the olivine *a* axis orientations to perpendicular to the mantle flow direction (Jung & Karato, 2001). This configuration is referred to as olivine type-B, whereas the relationship of dry olivine is type-A. In typical subduction zones, the mantle wedge tip meets the conditions for the existence of type-B olivine whereas type-A olivine is found throughout the mantle wedge core (Kneller et al., 2005). However, due to the young age (~14 Ma) of the Cocos plate and its high temperature (>900 °C), we can expect that most of the azimuthal anisotropy in the mantle wedge in central and southern Mexico is dominated by type-A olivine CPO (Bernal-López et al., 2016; Castellanos et al., 2017; Husker & Davis, 2009; Manea et al., 2005; Pardo & Suarez, 1995).

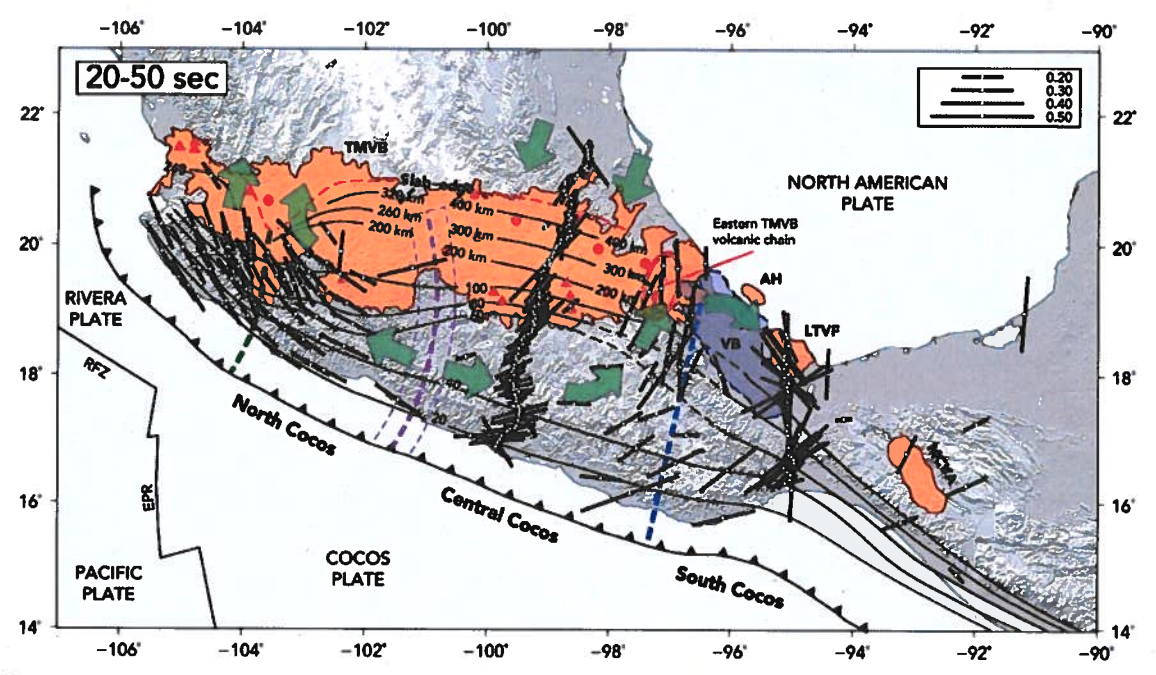


Figure 11. Map of the azimuthal anisotropy results for the lower crust and upper mantle. The orientation of the vectors give the seismically fast direction, ϕ , and the length of the lines is proportional to the amplitude of the anisotropy, A. The thick green arrows depict the possible trajectories of mantle flows inferred from our measurements. The red oval delimits the eastern TMVB volcanic chain.

Consistent with a previous anisotropy study of the region (Stubailo et al., 2012), our measurements show a preferential trench-parallel alignment of the seismically fast direction beneath the subducted slab in most of the forearc (Figure 11). However, our anisotropy map displays, for the first time, a well-defined flow pattern that supports the hypothesis of a slab tear in South Cocos. In the case of a slab tear or gap, mantle material could flow through the slab window and create the mantle fabric depicted by our anisotropic parameters. The variations in slab dip and rollback rate of the plate along the MAT would also induce a 3-D flow field, in which mantle materials move from beneath the slab to the mantle wedge underneath Veracruz. A similar type of flow in the Rivera-Cocos plate boundary has been proposed to control the asthenospheric anisotropy that is observed beneath the MARS and NARS seismic arrays (Soto et al., 2009; Yang et al., 2009), which would explain the subtle north-northeast rotation in our fast axes in the Rivera segment of the MAT. Our results cannot provide definite evidence for the slab tear that has been proposed to exist along the projection of the OFZ in western Mexico (Dougherty et al., 2012) as the seismic coverage around this area is sparse. Anisotropy in the backarc of central Mexico (i.e., the northern section of the MASE array), on the other hand, appears to be primarily controlled by a trench-perpendicular 2-D corner flow that is induced by the abrupt downdip motion of the slab (Bernal-López et al., 2016). Moreover, although outside the scope of this paper, the azimuthal anisotropy measurements for the upper crust display a consistent trench-parallel orientation regardless of the distance from the MAT, suggesting that anisotropy at this depth may be dominated by fractures subject to lateral compression (Figure S3).

3.3. The Eastern End of the TMVB

There has been significant progress in understanding the TMVB and the Central American subduction system. However, the nature of the pronounced change in arc volcanism in central and southern Mexico has remained ambiguous. On the basis of structural arguments, our study indicates that a tear in the South Cocos slab can explain most of the enigmatic features that characterize this segment of the MAT (Figure 12). For the remainder of this paper, we will refer to the northern part of South Cocos as Central Cocos whereas the slab segment that is south of the possible tear will remain as South Cocos.

The first piece of evidence for a possible slab tear separating Central and South Cocos comes from geomorphological features. The general extent of the NNE volcanic chain at the easternmost TMVB suggests that this composite structure is linked to a source of magma and fluids that reached the surface in a linearly distributed

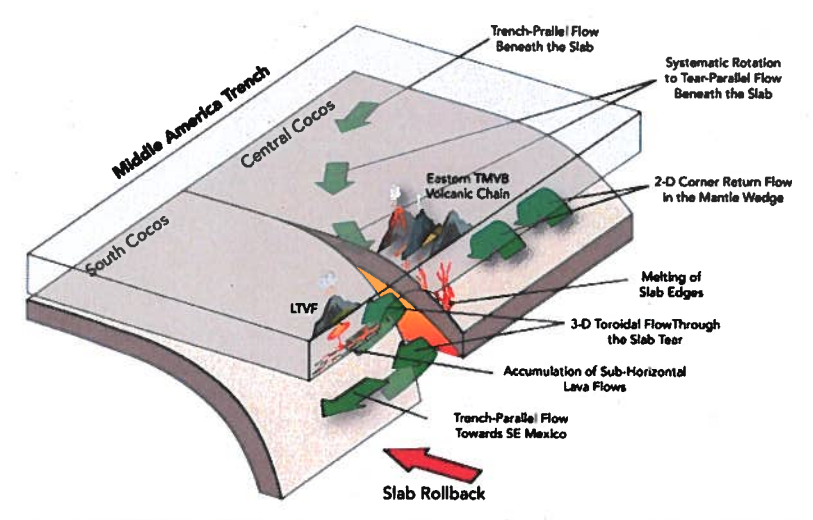


Figure 12. Three-dimensional schematic illustration of the proposed tectonic setting and inferred mantle flow (green arrows). Asthenospheric mantle materials are flowing almost trench-parallel beneath the slab in the forearc region until they are redirected to the mantle wedge through a tear that separates Central and South Cocos. The accelerated rollback rate of South Cocos relative to Central Cocos introduces a suction force that further displaces the mantle materials laterally toward the south of Mexico. The shear stress exerted by the toroidal flow around the slab tear may be transporting the melts and fluids that are feeding the volcanoes in the LTVF from central Mexico, thus allowing their existence without any slab material at an appropriate depth directly underneath them. Some of the active volcanoes composing the eastern TMVB volcanic chain, however, might still be fed by some slab edge melting mechanism.

Anisotropy in the backarc of central Mexico (i.e., Central Cocos) is primarily controlled by a trench-perpendicular 2-D corner flow that is induced by the downdip motion of the slab. The flow of mantle materials through a slab tear, with the accompanying slab edge melting, may explain the exceptional spatial distribution of stratovolcanoes in the eastern sector of the TMVB, as well as the abrupt change in the source of melts observed in young rocks in this segment of the MAT. The eye in Figure 1 marks the viewpoint of the observer.

order. This narrowly localized source of melts may have been associated with an upwelling of the isotherms due to the asthenospheric mantle material flowing around the edge of the slab during tear propagation, a mechanism similar to the one that formed the cross-back-arc volcanic trail in the Ryukyu subduction zone in Japan (Lin et al., 2004). There is also a systematic southward progression in age along the volcanic chain (Ferrari et al., 2012), which is characteristic of plate rollback and/or tear development (Dilek & Altunkaynak, 2009). However, Siebert and Carrasco-Núñez (2002) report the presence of young basaltic rocks in the northem part of the chain. The chronological similarity between the activity at the current volcanic front and in the back-arc region suggests that volcanism is controlled not only by regular subduction and rollback but also by a mechanism, such as an elongated slab window, that could allow melts to reach the backarc at a relatively contemporary time. Moreover, Gómez-Tuena et al. (2003) suggest that the dramatic change in the composition of volcanic rocks in the easternmost TMVB is associated to a gradual increase in the angle of subduction at the end of the Miocene, which would allow the partial melting of a relatively deeper mantle source. Nonetheless, the flow of mantle materials through a slab tear, with the accompanying slab edge melting, may also explain the acute change in the source of melts and the adaktic signature observed in young rocks in the eastern sector of the TMVB (e.g., Davies & von Blanckenburg, 1995; Guivel et al., 2006; Ribeiro et al., 2016). We suggest that the building of the volcanic chain in the eastern TMVB represents an early stage of the slab tear

The abrupt termination of the TMVB at its eastern end, and the resulting discontinuity of arc volcanism, introduces complexity into the slab tear hypothesis but does not abate it. To explain the absence of surficial volcanism directly in the coastal Veracruz basin, Dougherty and Clayton (2014) suggest that the tear is a less developed or young feature located in the downdip portion of the slab, and that consequently any material flowing through it is not rising to a sufficiently shallow depth to have an effect on the overriding plate. We propose a slightly different scenario. Rather than the tear being underdeveloped, we hypothesize that the rapid rollback rate of South Cocos relative to Central Cocos, accelerated by the influx of less dense asthenosphere material into the mantle wedge through the slab window (Schellart et al., 2007; Soto et al., 2009), introduces



a suction force that increases the strength of the toroidal flow through the tear and drags the mantle materials under Central Cocos laterally toward the south of Mexico. As a result, any material flowing through the tear is unable to reach the surface directly at the Veracruz basin. The main evidence for this scenario comes from the azimuthal anisotropy results (Figure 11), where the asthenospheric mantle appears to be flowing almost trench-parallel beneath the slab until it flows out into the mantle wedge through the possible tear and heads toward southeastern Mexico. The subtle interruption in the radial anisotropy pattern at the eastern end of the TMVB (Figure 10) also suggests the dominance of a horizontal mantle flow in the presence of a weak and localized vertical flow just where the tear is proposed to be. Furthermore, we suggest that some of the active volcanoes of the eastern TMVB volcanic chain are still being fed by some slab edge melting mechanism, and that the southeastern drag of mantle materials below the Veracruz area is responsible for the isolated volcanic expressions that are present in central and southern Mexico. As described earlier, there is no deep source of melts feeding the LTVF in the same way that we observe for the TMVB in central Mexico (Figure 6). Instead, there is a strong positive radial anisotropy, indicative of accumulation of horizontal or subhorizontal lava flows, that appears to be transporting the magma that is building the volcanoes at the LTVF. We suggest that the shear stress exerted by the toroidal flow around the slab tear is responsible for orienting the magma flow horizontally and that the melts are then able to reach the surface through a series of vertically oriented conduits that are just below the LTVF. This scenario is similar to the process that created Mount Etna in Europe (Gvirtzman & Nur, 1999) and would explain the younger age of LTVF magmas (7 Ma) relative to the overall age of the TMVB (Nelson & González-Caver, 1992). The horizontal transport of mantle material in the uppermost mantle and lower crust underneath the Veracruz basin is further supported by geochemical data that advocates that the LTVF source is likely to reside in the lithosphere rather than the asthenosphere, and would also explain why the LTVF evolved magmas do not require a slab component in their genesis (Verma, 2006). A similar scenario, in which the anomalous setting of the southern Mexico volcanism is related to a mantle flow readjustment, was proposed by Manea et al. (2013). However, different from this study, Manea et al. (2013) argues that materials in the mantle wedge are being pushed laterally out of central Mexico due to the ongoing slab flattening process, and that the combination of this flow with a decrease in temperature around the flat-slab area may be responsible for the discontinuity of arc volcanism.

Even though the slab flattening in central Mexico can also provide a plausible explanation for the spatial variation of the volcanic arcs, the idea of a slab tear and a perturbed mantle wedge underneath the Veracruz basin is more appealing for two main reasons. First, the influx of hot, less dense asthenospheric mantle material flowing through the tear to the Veracruz area may explain how the contrasting topographic relief between the eastern TMVB and coastal Veracruz basin is supported by the variations in the crustal thicknesses. Second, the temperature change introduced by the hot mantle flow may significantly influence the thermomechanical state of the subducting slab and explain the abrupt termination of the seismicity associated with the Cocos plate at the southern end of the Veracruz basin (Figures S4 and S5). Among the many hypotheses put forward to explain the occurrence of intermediate-depth earthquakes, dehydration embrittlement (Kirby et al., 1996), which is the brittle failure associated with dehydration reactions of hydrous minerals in the slab and upper mantle, is considered to be the leading mechanism (Wang et al., 2017). This hypothesis asserts that intermediate-depth earthquakes occur in subducting slabs where dehydration is expected but are absent from parts of the slab predicted to be anhydrous (Hacker et al., 2003). To this day, a direct link between lithospheric tearing and intermediate-depth seismicity has not been established. Meighan et al. (2013) report a positive correlation between slab tears and intermediate-depth seismicity and suggest that most of the seismic sequences that occur in these environments are associated with the fluid-related embrittlement of mantle rocks. However, we argue that, in the case of the subduction system in Mexico, the elevated rate of shear heating due to strong lateral mantle materials flowing through the tear has deprived northern South Cocos of most of the fluids stored in its crust. This, in turn, prevents intraplate earthquakes from occurring due to the absence of dehydration embrittlement at the northern South Cocos' intermediate depth. An alternate scenario that may explain the absence of subduction-related seismicity in the Veracruz region is slab detachment, which involves the detachment of a portion of the slab during ongoing subduction (Isacks & Molnar, 1969). However, the lack of a strong topographic response directly in the Veracruz basin (i.e., uplift) or any sharp lateral contrasts in the trench topography (Bottrill et al., 2012) suggests that an abrasive process such as slab break-off might not be responsible for the absence for seismicity and surface volcanism in this area. The exis-



tence of a horizontal separation of the two slab segments with a relatively large gap in between due to slab bending (Obayashi et al., 2009) may also explain the absence of intermediate-depth seismicity underneath Veracruz. Yet focal mechanisms of regional intraslab earthquakes do not show a trench-parallel trending *T* axis orientation along the sharp transition in slab dip (Dougherty & Clayton, 2014), suggesting that the tear, if existent, is more likely to be propagating vertically rather than horizontally. Note that both the down-dropped side of the slab (in the case of a vertically propagating tear) and a large horizontal gap between the slab segments could have created the topographic hole for the Veracruz basin, but only the vertically propagating tear scenario would explain the existence of the LTVF without a deep source of melts directly underneath the stratovolcanoes.

Slab tearing has been observed in numerous subduction systems around the world and is generally believed to be triggered by local collisional events (Sacks & Secor Jr, 1990) or by the variations in age, temperature, geometry, and convergence rate of the subducting plate along the trench (e.g., Govers & Wortel, 2005, and references therein). For the case of southern Mexico, Dougherty and Clayton (2014) suggest that the possible tear separating South and Central Cocos may be related to the subduction of several parallel ridges or topographic heterogeneities off the coast of Oaxaca or, alternatively, to the accommodation of strain due to the sharp change in slab geometry (or some combination of the two). Together with the slab window along the Rivera-Cocos plate boundary, and the tear in western Mexico, a tear in southern Mexico has important implications in the subduction dynamics of Central America. Aside from exerting strong influence on the surface volcanism, the composite mantle flow formed by the movement of asthenospheric mantle materials from the back to the front of the slab through the gap and tears may be allowing the separate segments of the Cocos plate to roll back independently and further promote the large variations in dip that characterize the Mexico subduction system (Dougherty & Clayton, 2014). Our proposed scenario wherein the hot, less dense asthenospheric mantle material is flowing through the tear to the Veracruz area is consistent with regional thermal models that suggest the existence of an upper mantle with relatively low density and high temperatures in southern Mexico (Goes & van der Lee, 2002). However, further heat flow measurements as well as geodynamical modeling of the mantle flow in this setting are required in order to provide more quantitative insights into the role of the slab tear in the Mexico subduction system.

4. Conclusions

We have used the discrepancy between Rayleigh and Love waves derived from ambient seismic noise cross correlations to develop high-resolution anisotropic images for central Mexico and showed that the transition from flat to steeper subduction is more likely to be accommodated by a slab tear than a sharp flexure. A 2-D profile of the radial anisotropy model along the MASE line shows apparent melt migration pathways that go from the steeply dipping portion of the subducted slab to a sill complex in the lower crust beneath the TMVB. Moreover, the flat portion of the slab appears to be dominated by vertically oriented structures, such as fluid-filled cracks, that may be functioning as the primary conduit for slab dehydration. Along the VEOX line, our images suggest that volcanoes at the LTVF are fed by lava flows that are subhorizontally transported in the lower crust. Our azimuthal anisotropy results indicate that mantle material flows trench-parallel underneath the slab until it is redirected to the mantle wedge through a possible tear that separates Central and South Cocos. The difference in the rollback rates of the plates introduces a suction force that further displaces the asthenospheric mantle material toward southern Mexico. We hypothesize that the shear stress exerted by this toroidal flow is transporting the lava flows from the slab window to the LTVF, and may also be responsible for the few other isolated volcanoes present in southern Mexico. The lack of subduction-related earthquakes underneath the Veracruz basin may therefore be explained by two plausible scenarios: (a) The elevated rate of shear heating due to the rapid influx of hot, less dense material flowing through the tear underneath Veracruz has depleted most of the fluids that were once stored in the slab's oceanic crust. As a result, intraplate earthquakes do not occur due to the absence of dehydration embrittlement at intermediate depths. (b) The tear is accommodated by a lateral movement promoted by slab bending such that there exists a relatively large gap in between the two slab segments underneath the Veracruz basin. Given that a large lateral slab gap beneath Veracruz would not explain the existence of the LTVF without a deep source of melts below the stratovolcanoes and that there appears to be no obvious topographic response to this process, we favor the first scenario over the second one.



Acknowledgments This research was supported by NSF, EAR-1645063 award. Our recognition is extended to the DGAPA-PAPIIT IN105816 and CONACYT 177676 projects for maintaining the GECO Network. Our recognition is extended to the DGAPA-PAPIIT IN 105816, CONACYT 270544, and CONACYT 177676 projects for financing and maintaining the GECO Network. SSN data were obtained by the Servicio Sismológico Nacional (México), and we thank its personnel for station maintenance, data acquisition, and distribution (SSN, 2017). We also thank the Centro de Ciencias de la Tierra de la Universidad Veracruzana (CCTUV) and the Civil Protection authorities of Veracruz (SPC-VER) for maintaining the UV network. We are grateful to Michael Brudzinski, Enrique Cabral-Cano, and Alejandra Arcinlega-Ceballos for providing access to OXNET data. We also thank the IRIS-PASSCAL Instrumentation Center for making the data available. Figures were made using the Generic Mapping Tools v.4.5.9 (www.soest.hawail.edu/gmt, last accessed November 2017; Wessel and Smith, 1998). We gratefully thank Zack Spica and Sara Dougherty for providing their insight and expertise throughout the development of this work. We are also very grateful to Martha Savage and two anonymous reviewers for their careful and constructive suggestions. The final shear wave velocity and radial anisotropy models can be downloaded from https://github.com/ JorgeCastillo90/Paper-2018JB015783R.git.

References

- Ammon, C. J., Kosarian, M., Herrmann, R. B., Pasyanos, M. E., Walter, W. R., & Tkalcic, H. (2004). Simultaneous inversion of receiver functions, multi-mode dispersion, and travel-time tomography for lithospheric structure beneath the Middle East and North Africa. In Chavez, F. C., Benson, J., Hanson, S., Mark, C., & Wetovsky, M. A. (Eds.), Proceedings of the 26th seismic research review—Trends in nuclear explosion monitoring. Los Alamos, New Mexico: Los Alamos National Laboratory, pp. 17–28.
- An, M., Wiens, D. A., Zhao, Y., Feng, M., Nyblade, A. A., Kanao, M., et al. (2015). S-velocity model and inferred Moho topography beneath the Antarctic plate from Rayleigh waves. *Journal of Geophysical Research*: *Solid Earth*, 120, 359–383. https://doi.org/10.1002/2014J8011332 Anderson, D. L. (1965). Recent evidence concerning the structure and composition of the earth's mantle. *Physics and Chemistry of the Earth*, 6, 1–131.
- Arroyo, I. G., Husen, S., Flueh, E. R., Gossler, J., Kissling, E., & Alvarado, G. (2009). Three-dimensional P-wave velocity structure on the shallow part of the central Costa Rican Pacific margin from local earthquake tomography using off-and onshore networks. Geophysical Journal International, 179(2), 827–849.
- Babuska, V., & Cara, M. (1991). Seismic anisotropy in the Earth, vol. 10, Netherlands: Springer Science & Business Media.
- Backus, G. (1970). A geometrical picture of anisotropic elastic tensors. Reviews of geophysics, 8(3), 633-671.
- Bandy, W., Hilde, T., & Yan, C. (2000). The Rivera-Cocos plate boundary: Implications for Rivera-Cocos relative motion and plate fragmentation. Geological Society of America Special Papers, 334, 1 – 28.
- Barmin, M., Ritzwoller, M., & Levshin, A. (2001). A fast and reliable method for surface wave tomography, in A. L. Levshin & M. H. Ritzwoller (Eds.), Manitaring the comprehensive nuclear-test-ban treaty: Surface waves. Basel: Springer, pp. 1351–1375.
- Bensen, G., Ritzwoller, M., Barmin, M., Levshin, A., Lin, F., Moschetti, M., et al. (2007). Processing seismic ambient noise data to obtain reliable broad-band surface wave dispersion measurements. Geophysical Journal International, 169(3), 1239–1260.
- Bernal-López, L. A., Garibaldi, B. R., Soto, G. L., Valenzuela, R. W., & Escudero, C. R. (2016). Seismic anisotropy and mantle flow driven by the Cocos slab under southern Mexico. Pure and Applied Geophysics, 173(10-11), 3373-3393.
- Blackman, D. K., & Kendell, J. (2002). Seismic anisotropy in the upper mantle 2. Predictions for current plate boundary flow models. Geochemistry, Geophysics, Geosystems, 3(9), 8602. https://doi.org/10.1029/2001GC000247
- Bottrill, A. D., van Hunen, J., & Allen, M. B. (2012). Insight into collision zone dynamics from topography: Numerical modelling results and observations. Solid Earth, 3(2), 387.
- Campillo, M., & Paul, A. (2003). Long-range correlations in the diffuse seismic coda. Science, 299(5606), 547-549.
- Castellanos, J., Pérez-Campos, X., Valenzuela, R., Husker, A., & Ferrari, L. (2017). Crust and upper-mantle seismic anisotropy variations from the coast to inland in central and southern Mexico. Geophysical Journal International, 210(1), 360-374.
- Córdoba Montiel, F., Iglesias Mendoza, A., Singh, S. K., Spica, Z., & Legrand, D. (2014). Tomografía de velocidad de grupo de ondas de rayleigh para el oriente de méxico y el istmo de tehuantepec. Boletín de la Sociedad Geológica Mexicana, 66(3), 441–457.
- Córdoba-Montiel, F., Iglesias, A., Pérez-Campos, X., Sieron, K., de Trabajo del Servicio Sismológico Nacional, G., Valdés-Goruzález, C., et al. (2018). The broadband seismological network of Veracruz, Mexico: Toward a regional seismotectonic interpretation. Seismological Research Letters, 89(2A), 345–355.
- Cruz-Atienza, V. M., Husker, A., Legrand, D., Caballero, E., & Kostoglodov, V. (2015). Nonvolcanic tremor locations and mechanisms in Guerrero, Mexico, from energy-based and particle motion polarization analysis. *Journal of Geophysical Research: Solid Earth*, 120, 275–289. https://doi.org/10.1002/2014/8011389
- Davies, J. H., & von Blanckenburg, F. (1995). Slab breakoff: A model of lithosphere detachment and its test in the magmatism and deformation of collisional orogens. Earth and Planetary Science Letters, 129(1-4), 85-102.
- Debayle, E., & Sambridge, M. (2004). Inversion of massive surface wave data sets: Model construction and resolution assessment. Journal of Geophysical Research, 109, B02316. https://doi.org/10.1029/2003JB002652
- Dement, A. (1978). Características del eje neovolcánico transmexicano y sus problemas de interpretación. Revista mexicana de ciencias geológicas, 2(2), 172–187.
- Dilek, Y. & Altumiaynak, Ş. (2009). Geochemical and temporal evolution of cenozoic magmatism in Western Turkey: Mantle response to collision, slab break-off, and lithospheric tearing in an orogenic belt. Geological Society, London, Special Publications, 311(1), 213–233.
- Dougherty, S. L., & Clayton, R. W. (2014). Seismicity and structure in central Mexico: Evidence for a possible slab tear in the South Cocos plate. Journal of Geophysical Research: Solid Earth, 119, 3424—3447. https://doi.org/10.1002/2013JB010883
- Dougherty, S. L., Clayton, R. W., & Helmberger, D. V. (2012). Seismic structure in central Mexico: Implications for fragmentation of the subducted Cocos plate. Journal of Geophysical Research, 117, 809316. https://doi.org/10.1029/2012JB009528
- Dziewonski, A. M., & Anderson, D. L. (1981). Preliminary reference earth model. *Physics of the Earth and Planetary Interiors*, 25(4), 297–356. Ekström, G., & Dziewonski, A. M. (1998). The unique anisotropy of the Pacific upper mantle. *Nature*, 394(6689), 168.
- Espindola, V. H., Quintanar, L., & Espindola, J. M. (2017). Crustal structure beneath Mexico from receiver functions. Bulletin of the Seismological Society of America, 107(5), 2427 – 2442.
- Fasola, S., Brudzinski, M. R., Ghouse, N., Solada, K., Sit, S., Cabral-Cano, E., et al. (2016). New perspective on the transition from flat to steeper subduction in Oazaca, Mexico, based on seismicity, nonvolcanic tremor, and slow slip. Journal of Geophysical Research: Solid Earth, 121, 1835—1848. https://doi.org/10.1002/2015/B012709
- Ferrari, L. (2004). Slab detachment control on mafic volcanic pulse and mantle heterogeneity in central Mexico. *Geology*, 32(1), 77–80. Ferrari, L., Orozco-Esquivel, T., Manea, V., & Manea, M. (2012). The dynamic history of the Trans-Mexican Volcanic Belt and the Mexico subduction zone. *Tectonophysics*, 522, 122–149.
- Ferrari, L., Petrone, C. M., & Francalanci, L. (2001). Generation of oceanic-island basalt-type volcanism in the western Trans-Mexican Volcanic Belt by slab rollback, asthenosphere infiltration, and variable flux melting. Geology, 29(6), 507 –510.
- Ferrarl, L., Tagamil, T., Eguchi, M., Orozco-Esquivel, M. T., Petrone, C. M., Jacobo-Alberrán, J., & López-martínez, M. (2005). Geology, geochronology and tectonic setting of late cenozoic volcanism along the southwestern Guff of Mexico: The eastern alkaline province revisited. *Journal of Volcanology and Geothermal Research*, 146(4), 284-306.
- Fouch, M. J., & Rondenay, S. (2006). Seismic anisotropy beneath stable continental interiors. Physics of the Earth and Planetary Interiors, 158(2-4), 292–320.
- Geite, B., Iglesias, A., Villaseñor, A., Herraiz, M., & Pacheco, J. F. (2012). Crustal structure of Mexico and surrounding regions from seismic ambient noise tomography. Geophysical Journal International, 188(3), 1413–1424.
- Gardner, G., Gardner, L., & Gregory, A. (1974). Formation velocity and density The diagnostic basics for stratigraphic traps. Geophysics, 39(6, 770–780.
- Goes, S., & van der Lee, S. (2002). Thermal structure of the North American uppermost mantle inferred from seismic tomography. *Journal of Geophysical Research*, 107(83), 2050. https://doi.org/10.1029/2000/B000049



- Gómez-Tuena, A., LaGatta, A. B., Langmuir, C. H., Goldstein, S. L., Ortega-Gutiérrez, F., & Carrasco-Núfiez, G. (2003). Temporal control of subduction magmatism in the eastern Trans-Mexican Volcanic Belt: Mantle sources, slab contributions, and crustal contamination. Geosystems, Geochemistry, Geophysics, 4(8), 8912. https://doi.org/10.1029/2003gc000524
- Górnez-Tuena, A., Orozoo-Esquivel, M. T., & Ferrari, L. (2006). Petrogé,nesis ígnea de la faja volcánica transmexicana. Boletín de la Sociedad Geológica Mexicana, 57(3), 227–283.
- Govers, R., & Wortel, M. (2005). Lithosphere tearing at step faults: Response to edges of subduction zones. Earth and Planetary Science Letters, 236(1-2), 505–523.
- Guivel, C., Morata, D., Pelleter, E., Espinoza, F., Maury, R. C., Lagabrielle, Y., et al. (2006). Miocene to Late Quaternary Patagonian basalts (46–47 s): Geochronometric and geochemical evidence for slab tearing due to active spreading ridge subduction. Journal of Volcanology and Geothermal Research, 149(3), 346–370.
- Gwirtzman, Z., & Nur, A. (1999). The formation of Mount Etna as the consequence of slab rollback. Nature, 401(6755), 782.
- Hacker, B. R., Peacock, S. M., Abers, G. A., & Holloway, S. D. (2003). Subduction factory 2. Are intermediate-depth earthquakes in subducting slabs linked to metamorphic dehydration reactions? *Journal of Geophysical Research*, 108(B1), 2030. https://doi.org/10.1029/2001jb001129
- Haney, M. M., Mikesell, T. D., von Wijk, K., & Nakahara, H. (2012). Extension of the spatial autocorrelation (SPAC) method to mbted-component correlations of surface waves. Geophysical Journal International, 191(1), 189–206.
- Harmon, N., Gerstoft, P., Rychert, C. A., Abers, G. A., Salas de La Cruz, M., & Fischer, K. M. (2008). Phase velocities from seismic noise using bearnforming and cross correlation in Costa Rica and Nicaragua. Geophysical Research Letters, 35, L19303, https://doi.org/10.1029/2008GL035387
- Husen, S., Quintero, R., Kissling, E., & Hacker, B. (2003). Subduction-zone structure and magmatic processes beneath Costa Rica constrained by local earthquake tomography and petrological modelling. Geophysical Journal International, 155(1), 11-32.
- Husker, A., & Davis, P. M. (2009). Tomography and thermal state of the Cocos plate subduction beneath Mexico city. Journal of Geophysical Research, 114, B04306. https://doi.org/10.1029/2008/B006039
- Husker, A. L., Kostoglodov, V., Cruz-Atienza, V. M., Legrand, D., Shapiro, N. M., Payero, J. S., et al. (2012). Temporal variations of non-volcanic tremor (NVT) locations in the Mexican subduction zone: Finding the NVT sweet spot. Geochemistry, Geophysics, Geosystems, 13, Q03011. https://doi.org/10.1029/2011GC003916
- Isacks, B., & Molnar, P. (1969). Mantle earthquake mechanisms and the sinking of the lithosphere. Nature, 223(5211), 1121.
- Jaxybulatov, K., Shapiro, N., Koulakov, I., Mordret, A., Landès, M., & Sens-Schönfelder, C. (2014). A large magmatic sill complex beneath the Toba caldera. Science, 346(6209), 617–619.
- Jödicke, H., Jording, A., Ferrari, L., Arzate, J., Mezger, K., & Rüpke, L. (2006). Fluid release from the subducted Cocos plate and partial melting of the crust deduced from magnetotelluric studies in southern Mexico: Implications for the generation of volcanism and subduction dynamics. Journal of Geophysical Research, 111, 808102. https://doi.org/10.1029/2005/8003739
- Jung, H., & Karato, S.-I. (2001). Water-induced fabric transitions in olivine. Science, 293(5534), 1460-1463.
- Kim, Y., Clayton, R., & Jackson, J. (2010). Geometry and seismic properties of the subducting Cocos plate in central Mexico. Journal of Geophysical Research, 115, B06310. https://doi.org/10.1029/2009JB006942
- Kim, Y., Clayton, R. W., & Kepple, F. (2011). Evidence of a collision between the Yucatán Block and Mexico in the Miocene. Geophysical Journal International, 187(2), 989-1000.
- Kirby, S., Engdahl, R. E., & Denlinger, R. (1996). Intermediate-depth intraslab earthquakes and arc volcanism as physical expressions of crustal and uppermost mantle metamorphism in subducting slabs. In G. E. Bebout et al. (Eds.), Subduction top to bottom (pp. 195–214). Washington, DC: American Geophysical Union.
- Kneller, E. A., Van Keken, P. E., Karato, S.-I., & Park, J. (2005). B-type olivine fabric in the mantle wedge: insights from high-resolution non-Newtonian subduction zone models. Earth and Planetary Science Letters, 237(3-4), 781–797.
- Lin, J.-Y., Hsu, S.-K., & Sibuet, J.-C. (2004). Melting features along the western Ryukyu slab edge (northeast Taiwan): Tomographic evidence. Journal of Geophysical Research, 109, B12402. https://doi.org/10.1029/2004JB003260
- Lobkis, O. I., & Weaver, R. L. (2001). On the emergence of the Green's function in the correlations of a diffuse field. The Journal of the Acoustical Society of America, 110(6), 3011–3017.
- Luo, Y., Yang, Y., Xu, Y., Xu, H., Zhao, K., & Wang, K. (2015). On the limitations of interstation distances in ambient noise tomography. Geophysical Journal International, 201(2), 652–661.
- Ma, Y., & Clayton, R. W. (2014). The crust and uppermost mantle structure of southern Peru from ambient noise and earthquake surface wave analysis. Earth and Planetary Science Letters, 395, 61 – 70.
- Mainprice, D., & Ildefonse, B. (2009). Seismic anisotropy of subduction zone minerals—Contribution of hydrous phases. In S. Lallemand & F. Funkclelo (Eds.), Subduction zone geodynamics. Verlag, Berlin-Heidelberg: Springer, pp. 63 84.
- Manea, V. C., Manea, M., & Ferrari, L. (2013). A geodynamical perspective on the subduction of Cocos and Rivera plates beneath Mexico and Central America. *Tectonophysics*, 609, 56–81.
- Manea, V. C., Manea, M., Kostoglodov, V., & Sewell, G. (2005). Thermo-mechanical model of the mantle wedge in central Mexican subduction zone and a blob tracing approach for the magma transport. Physics of the Earth and Planetary Interiors, 149(1-2), 165 – 186.
- Meighan, H. E., Brink, U., & Pulliam, J. (2013). Slab tears and intermediate-depth seismicity. Geophysical Research Letters, 40, 4244—4248. https://doi.org/10.1002/grl.50830
- Melgar, D., & Pérez-Campos, X. (2011). Imaging the Moho and subducted oceanic crust at the isthmus of Tehuantepec, Mexico, from receiver functions. Pure and applied geophysics, 168(8-9), 1449-1460.
- Molina-Garza, R., & Umutia-Fucugauchi, J. (1993). Deep crustal structure of central Mexico derived from interpretation of Bouguer gravity anomaly data. Journal of Geodynamics, 17(4), 181 – 201.
- Mult, J. B., & Tsal, V. C. (2017). Rayleigh-wave H/V via noise cross correlation in Southern California. Bulletin of the Seismological Society of America, 107(5), 2021 – 2027.
- Nelson, S. A., & González-Caver, E. (1992). Geology and K-Ar dating of the Tuxtla Volcanic Field, Veracruz, Mexico. Bulletin of Volcanology, 55(1-2), 85-96.
- Nelson, S. A., Gonzalez-Caver, E., & Kyser, T. K. (1995). Constraints on the origin of alkaline and calc-alkaline magmas from the Tuxtia Volcanic Field, Veracruz, Mexico. Contributions to Mineralogy and Petrology, 122(1-2), 191 211.
- Nicolas, A., & Christensen, N. I. (1987). Formation of anisotropy in upper mantle peridotites—A review. In K. Fuchs & C. Froidevaux (Eds.), Composition, structure and dynamics of the lithosphere-asthenosphere system. Washington, D.C. American Geophysical Union, pp. 111–123.
- Obayashi, M., Yoshimitsu, J., & Fukao, Y. (2009). Tearing of stagmant slab. Science, 324(5931), 1173-1175.



- Pardo, M., & Suarez, G. (1995). Shape of the subducted Rivera and Cocos plates in southern Mexico: Seismic and tectonic implications. Journal of Geophysical Research, 100(87), 12,357–12,373.
- Pérez-Campos, X., Espindola, V. H., Pérez, J., Estrada, J. A., Monroy, C. C., Bello, D., et al. (2018). The Mexican national seismological service. An overview, Seismological Research Letters, 89(2A), 318-323.
- Pérez-Campos, X., Kim, Y., Husker, A., Davis, P. M., Clayton, R. W., Iglesias, A., et al. (2008). Horizontal subduction and truncation of the Cocos plate beneath central Mexico. Geophysical Research Letters, 35, L18303. https://doi.org/10.1029/2008GL035127
- Pham, T.-S., Tkalčić, H., Sambridge, M., & Kennett, B. L. (2018). Earth's correlation wavefield: Late coda correlation. Geophysical Research Letters, 45, 3035–3042. https://doi.org/10.1002/2018GL077244
- Ribeiro, J. M., Maury, R. C., & Grégoire, M. (2016). Are adakites slab melts or high-pressure fractionated mantle melts? Journal of Petrology, 57(5), 839–862.
- SSN (2017). Servicio Sismológico Nacional, instituto de Geoffsica, Universidad Nacional Autónoma de México, México. https://doi.org/10.21766/SSNMX/SN/MX
- Sacks, P. E., & Secor Jr, D. T. (1990). Delamination in collisional orogens. Geology, 18(10), 999-1002.
- Sager, K., Boehm, C., Ermert, L., Krischer, L., & Fichtner, A. (2018). Sensitivity of seismic noise correlation functions to global noise sources. Journal of Geophysical Research: Solid Earth. https://doi.org/10.1029/2018J8016042
- Schellart, W., Freeman, J., Stegman, D., Moresi, L., & May, D. (2007). Evolution and diversity of subduction zones controlled by slab width. Nature, 446(7133), 308.
- Shapiro, N. M., & Campillo, M. (2004). Emergence of broadband Rayleigh waves from correlations of the ambient seismic noise. Geophysical Research Letters, 31, L07614. https://doi.org/10.1029/2004GL019491
- Slebert, L., & Carrasco-Núñez, G. (2002). Late Pleistocene to precolumbian behind-the-arc matic volcanism in the eastern Mexican Volcanic Belt; Implications for future hazards. Journal of Volcanology and Geothermal Research, 115(1), 179–205.
- Smith, M. L., & Dahlen, F. (1973). The azimuthal dependence of love and Rayleigh wave propagation in a slightly anisotropic medium. Journal of Geophysical Research, 78(17), 3321–3333.
- Snieder, R. (2004). Extracting the Green's function from the correlation of coda waves: A derivation based on stationary phase. Physical Review E, 69(4), 046610.
- Soto, G. L., Ni, J. F., Grand, S. P., Sandvol, E., Valenzuela, R. W., Speziale, M. G., et al. (2009). Mantle flow in the Rivera Cocos subduction zone. Geophysical Journal International, 179(2), 1004–1012.
- Spica, Z., Perton, M., Calò, M., Legrand, D., Córdoba-Montiel, F., & Iglesias, A. (2016). 3-D shear wave velocity model of Mexico and South US: Bridging seismic networks with ambient noise cross-correlations (C¹) and correlation of coda of correlations (C³). Geophysical Journal International, 206(3), 1795 – 1813.
- Spica, Z., Perton, M., & Legrand, D. (2017). Anatomy of the Colima voicano magmatic system, Mexico. Earth and Planetary Science Letters, 459, 1-13.
- Stubailo, L, Beghein, C., & Davis, P. (2012). Structure and anisotropy of the Mexico subduction zone based on Rayleigh-wave analysis and implications for the geometry of the Trans-Mexican Volcanic Belt. *Journal of Geophysical Research*, 117, 805303. https://doi.org/10.1029/2011JB008631
- Suárez, G., & Sánchez, O. (1996). Shallow depth of seismogenic coupling in southern Mexico: Implications for the maximum size of earthquakes in the subduction zone. *Physics of the Earth and Planetary Interiors*, 93(1-2), 53–61.
- Syracuse, E. M., Abers, G. A., Fischer, K., MacKenzie, L., Rychert, C., Prottil, M., et al. (2008). Seismic tomography and earthquake locations in the Nicaraguan and Costa Rican upper mantile. Geochemistry, Geophysics, Geosystems, 9, Q07508. https://doi.org/10.1029/2008GC001963 Urrutia-Fucugauchi, J., & Flores-Ruiz, J. H. (1996). Bouguer gravity anomalies and regional crustal structure in central Mexico. International Geology Review, 38(2), 176–194.
- Verma, S. P. (2006). Extension-related origin of magmas from a garnet-bearing source in the Los Tuxtias voicanic field, Mexico. International Journal of Earth Sciences, 95(5), 871.
- Walker, K. T., Nyblade, A. A., Klemperer, S. L., Boltelmann, G. H., & Owens, T. J. (2004). On the relationship between extension and anisotropy: Constraints from shear wave splitting across the East African plateau. *Journal of Geophysical Research*, 109, 808302. https://doi.org/10.1029/2003J8002866
- Wang, J., Zhao, D., & Yao, Z. (2017). Seismic anisotropy evidence for dehydration embrittlement triggering intermediate-depth earthquakes. Scientific Reports, 7(1), 2613.
- West, J. D., Fouch, M. J., Roth, J. B., & Elkins-Tanton, L. T. (2009). Vertical mantle flow associated with a lithospheric drip beneath the great basin. Nature Geoscience, 2(6), 439.
- Yang, T., Grand, S. P., Wilson, D., Guzman-Speziale, M., Gomez-Gonzalez, J. M., Dominguez-Reyes, T., & Ni, J. (2009). Seismic structure beneath the Rivera subduction zone from finite-frequency seismic tomography. *Journal of Geophysical Research*, 114, 801302. https://doi.org/10.1029/2008JB005830
- Yao, H., van Der Hilst, R. D., & De Hoop, M. V. (2006). Surface-wave array tomography in SE Tibet from ambient seismic noise and two-station analysis I. Phase velocity maps. Geophysical Journal International, 166(2), 732—744.